# Theoretical model for subsurface microstructure prediction in micro-machining Ti-6Al-4V alloy - Experimental validation

Jinxuan Bai[1, 2], Qingshun Bai[1*], Zhen Tong[3], Hui Guo[1]

*1 School of Mechanical and Electrical Engineering, Harbin Institute of Technology, Harbin 150001, China*

*2 School of Mechanical Engineering, Purdue University, West Lafayette 47907, US*

*3 EPSRC Future Metrology Hub, Centre for Precision Technologies, University of Huddersfield, Huddersfield HD1 3DH, UK*

*\*Corresponding author*: qshbai@hit.edu.cn

**Abstract**: In this study, a new multiscale framework based on 2.5D discrete dislocation dynamics is proposed to predict the subsurface damaged layer evolution in micro-milling titanium alloy Ti-6Al-4V. This model takes into account the characteristics of component microstructure transformation and grain refinement by tracking the movement of matrix defects such as multiplication, slip, climb, cross-slip, junction and annihilation. Meanwhile, to understand the size dependence effect in micro-machining operation, a novel finite element orthogonal cutting model with dislocation density-based strain gradient constitutive equation is proposed and applied to reveal the far-field solution of driving stress of subsurface defect. The subsurface damaged layer characteristics including dislocation distribution and microstructure alteration of Ti-6Al-4V under various cutting conditions are studied with qualitative and quantitative assessment. The effects of processing parameters on subsurface features are analyzed. The obtained results have been compared with experimental findings utilizing the X-ray diffraction tests for validation purpose.

**Keywords:** micro-machining; subsurface damaged layer; dislocation dynamics; strain gradient; Ti-6Al-4V alloy

## 1 Introduction

Due to the characteristics of low density, high strength, unique corrosion resistance and excellent thermostability, titanium alloy Ti-6Al-4V micro-components find application in aerospace, mechanical electronic and biomedical industries [1, 2]. As a necessary means of microstructure manufacturing, ultra-precision milling technique has been the foundation for fabricating miniaturization component with complex surface features [3]. However, in comparison to conventional operations, the service performance of micro-component is not only on surface integrity but depends on the characteristic of subsurface damaged (SSD) layer [4]. During micro-cutting process, the SSD layer directly influences surface finish and dimensional precision, and even impacts on the mechanical properties and lifetime of workpiece [5]. Actually, the SSD layer can be regarded as the result of individual or combined effects of structural transformation induced by residual stresses [6], transmutation of crystal structure [7] and foreign bodies embedded [8]. Particularly, processing parameters always affect the intensity of above impacts and ultimately the distribution, thickness together with type of evoked subsurface organization. In this context, comprehensive understanding of the correlation mechanism among size effect, minimum chip thickness, cutting speed and induced SSD layer is a basic approach towards improving the performance of microfabrication.

An entire finished surface is comprised of several components: surface metamorphic layer, subsurface damaged layer and bulk material. Yan et al. [9] analyzed the formation mechanism of subsurface defects by using cross-sectional transmission electron microscope (XTEM) method in micro-cutting monocrystal silicon. The micrographs extracted from samples indicated that a thin amorphization layer was formed on the top of machined surface, below which was subsurface zone with a mass of dislocations occurred extending downwards. Ni et al. [10] asserted that the orthogonal machining process of commercially pure copper could produce mixed dislocation cell structures with intertwined damages in subsurface zone. Furthermore, Thomas et al. [11] investigated the influence of plastic strain on machined subsurface layer following high-speed milling operations. Ginting and

Nouari [12] accounted for the dependence of subsurface morphologies on milling speed and feed direction in dry machining titanium alloy. On the basic of electron backscatter diffraction (EBSD) technique, Touazine et al. [13] sought to achieve the accurate determination of damaged zone in Inconel 718 bulk material. Obtained misorientation maps demonstrated that a distortion deformation layer was present below the surface nearby carbides or twin boundaries. What is worth noting that the aforementioned experimental conclusions provided insufficient data on characterizing method of affected subsurface area and often, the introduced preparation damages were hardly distinguishable from the actual injury. Therefore, in order to investigate the correlations between machining parameters and subsurface organizations more precisely and efficiently, researchers have attempted to develop the forecasting model to simulate the microstructure transformation of SSD layer.

Dandekar et al. [14] proposed a multi-step finite element (FE) prediction model to accommodate for subsurface microstructure after processing aluminum matrix composite. Both simulation and experiment concluded that the depth of damaged layer increased with the rise of external cutting force. Moreover, this proposed model was used to assess the SSD layer evolution of brittle materials associated with high-speed grinding [15]. This investigation concentrated upon the influence of grinding speed, depth and abrasive grain structure on workpiece morphologies. However, the size effect contributes to absolutely difference in the principal removal mechanism of material around cutting edge between microfabrication and conventional manufacturing method. Thus, the institutional analytical or numerical models downsized from macro-machining were not available [16]. In addition, Shin and Ding. [17, 18] developed a new material equation for simulating chip generation mechanism as well as grain refinement process. But some parameters in their constitutive model were simply calibrated according to the stress-strain relationship obtained from corresponding Johnson-Cook material model, which cannot calculate the evolution of workpiece dislocation density accurately, let alone tracked dislocation position precisely. Recently, large-scale molecular dynamics (MD) simulation was adopted to obtain the pattern of crystal defects during nano-cutting process. Wang et al. [19] employed 3-dimensional MD approach to reveal the subsurface damages distribution in orthogonal cutting single crystal copper. The forming processes of machined surface and subsurface were revealed by investigating atomic migration. According to massively parallel processing technique, Pei et al. [20] accounted for the changes of cutting force, dislocation movement and substrate deformation under various cutting parameters. However, the heavy computational burden of MD significantly restricts the simulation scale, which not only incapable to calculate the interaction among numerous subsurface defects but also may suppress dislocation multiplication nearby grain boundaries.

When subsurface crystalline material deforms plastically, substrate damages could be known as dislocation nucleation and propagation. Accordingly, the overall mechanical properties of SSD layer are determined by above dislocation movement and interaction. Discrete dislocation dynamics (DDD) is a mesoscopic computer simulation technique that aims at gaining insights concerning subsurface dislocation configurations and mechanical properties. Ren et al. [21] applied DDD simulation on GH2035 alloy to investigate the dislocation patterns and microstructure morphologies during laser shock processing (LSP). The results indicated that substrate dislocation density had significantly dependence on external loading intensity. Zhang et al. [22] used the dynamic DDD simulations to complement static nano-indentation experiments. The 3-dimensional geometric construction was investigated with respect to dislocation forming mechanism. Bai et al. [23] proposed a multiscale discrete dislocation plastic (MDDP) framework to model dislocation patterns and strain responses in milling monocrystal silicon. In this research, the strain gradient material model was proposed to solve the far-field driving load of workpiece subsurface dislocation. An anisotropic 2.5-dimensional dislocation dynamics-based numerical framework developed for micro-cutting was conducted to characterize the distribution and alteration of substrate dislocation configurations qualitatively and quantitatively. The formation mechanism of SSD layer was elucidated from dislocation evolution, which exists in bulk material after cutting. Then, the influence of primary machining parameters on resultant microstructure were

captured to great details.

## 2 Dislocation density-based strain gradient constitutive equation

During ultra-precision cutting process, tool cutting edge radius is at the same level as the grain size of workpiece material. However, the substantial decline in the ratio of cutting edge radius and grain size fundamentally changed the effective rake angle in the contact zone of tool and workpiece, which was indicated as micro-cutting size effect. As shown in Fig.1, the rake angle $\alpha_t$ decided by equivalent shearing plane leads to a transformation from conventional shear action to plastic extrusion deformation, which borders on circular micro-indentation extrusion operation [24].
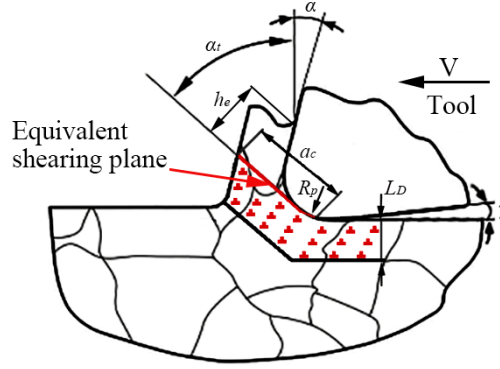


Figure 1. Plastic removal manner in micro-cutting titanium alloy Ti-6Al-4V. $\alpha_t$ is the effective rake angle, $\alpha$ is the physical rake angle, $\alpha_c$ is the length of equivalent shearing plane, $h_e$ is the extrusion depth of micro-cutter, and $t$ is the average thickness of dislocations layer. The red symbols denote the dislocations in chip and subsurface [3].

On the basis of Swadener et al. [25], the hardness $H$ in micro-scale is provided as following equation:

$$\frac{H}{H_0} = \sqrt{1 + \frac{R^*}{R_p}} \tag{1}$$

where $H_0$ is the macroscopic hardness, $R^*$ is characteristic length and $R_p$ is the radius of tool cutting edge. The $R^*$ and $R_p$ follow different routes and can be expressed by equation (2) and (3), respectively.

$$R^* = \frac{\bar{r}}{b\rho_{SSD}} \tag{2}$$

$$R_p = \frac{1}{b\rho_{GND}} \tag{3}$$

where $\bar{r}$ is Nye factor, $b$ is Burgers vector, $\rho_{SSD}$ is the density of statistically stored dislocations, and $\rho_{GND}$ is the density of geometrically necessary dislocations. According to equations (1) to (3) and Tabor factor of $H=3\sigma$ [26], the hardness can be related to flow stress.

$$\sigma = \sigma_0 \sqrt{1 + \bar{r}\frac{\rho_{GND}}{\rho_{SSD}}} \tag{4}$$

where $\sigma_0$ is determined by conventional Johnson-Cook (J-C) constitutive model. Considering the inhomogeneous distribution of dislocations in cell structure, a correction factor $\mu$ is introduced to properly state the changing mechanism of defect's quantity.

$$\sigma = \sigma_0 \sqrt{1 + \bar{r}\left(\frac{\rho_{GND}}{\rho_{SSD}}\right)^\mu} \tag{5}$$

In particular, $\rho_{SSD}$ is given by Taylor model.

$$\rho_{SSD} = \left(\frac{(A+B\varepsilon^n)\left(1+Cln\frac{\dot{\varepsilon}}{\dot{\varepsilon}_0}\right)(1-(T^*)^m)}{3\alpha Gb}\right)^2 \tag{6}$$

where $\alpha$ is constant and $G$ is shear modulus. On the basic of Fig.1, the geometrically necessary dislocations density

nearby tool tip can be calculated by equation (7).

$$\rho_{GND} = \frac{N_{GND}}{A_{GND}} = \frac{\frac{2h_e}{b}}{a_c t} = \frac{2h_e}{a_c L_D b} \tag{7}$$

Therefore, the dislocation density evolution in micro-cutting could be integrated with material constitutive equation as following:

$$\sigma = (A + B\varepsilon^n)\left(1 + Cln\frac{\dot{\varepsilon}}{\dot{\varepsilon}_0}\right)(1 - (T^*)^m)\sqrt{1 + \bar{r}\left(\frac{18a^2G^2bh_e}{\left(\left(A+B\varepsilon^n\right)\left(1+Cln\frac{\dot{\varepsilon}}{\dot{\varepsilon}_0}\right)(1-(T^*)^m)\right)^2 L_D a_c}\right)^\mu} \tag{8}$$

In comparison to former strain gradient models [27, 28], which introduces a length scale coefficient, equation (8) concentrates on the dislocation flow around cutting edge in extrusion operations. During micro-cutting process, the chips flowing would take place in nominal rake face if the undeformed chip thickness $h$ is less than the critical undeformed chip thickness $h_c$, $h_c= R_P (1+\sin(\alpha))$. Hence the ratio of $\alpha_c$ to $h_e$ is predicted as a function of tool effective rake angle $\alpha_t$. Otherwise, the extrusion depth of $h_e$ may be estimated to be nearly shearing plane length $\alpha_c$.

$$\frac{h_e}{a_c} = \tan(a_t) \qquad h < h_c \tag{9}$$

$$\frac{h_e}{a_c} = 1 \qquad h > h_c \tag{10}$$

where $\alpha_t$ is governed by equation (11) [29].

$$a_t = \arcsin\left(\frac{h}{R_p} - 1\right) \tag{11}$$

For validating its correctness and practicability, the strain gradient material plasticity model was programed by MATLAB®. Then, the stress-strain relationship predicted by equation (8) was contrasted with the predictions of flow stress data obtained by Johnson-Cook model for Ti64, Copper and 422ss in Fig. 2a. Meanwhile, this model has been used to reveal the temperature sensitivity, and Fig. 2b showed the materials mechanical responses of Copper for cutting temperature increased from 25° to 750°. Some materials parameters used in above comparisons were shown in Table 1 [28, 30]. Based on former studies [4, 7], the depth of subsurface dislocations layer $L_D$ seems to be bound up with machining parameters, which was considered as the depth of cut in this manuscript. Moreover, the Nye factor was introduced to measure the density of geometrically necessary dislocations in polycrystalline materials accurately, which is 1.85 for FCC metal and 1.0 for HCP material [31]. From Fig. 2a, it was found that the developed constitutive equation could predict higher flow stresses by considering cutting edge size effect for the temperature of 250 °C, strain rate of 1000/s, undeformed chip thickness of 10μm and effective rake angle of 30°. Fig. 2b suggested that the stress-strain behaviors which predicted strain gradient-based plasticity model can reasonably replicate the thermal softening effect at different cutting temperatures.
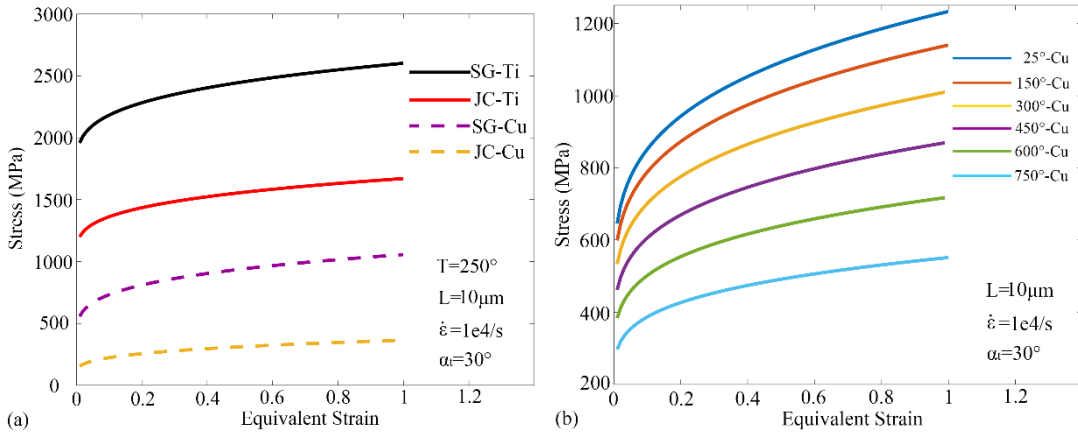

(a)


(b)

Figure 2. (a) J-C and strain gradient constitutive behaviors of Ti-6Al-4V and Copper. J-C denotes Johnson-Cook constitutive behavior and SG denotes dislocation theory-based strain gradient constitutive behavior. (b) strain gradient model predictions for Copper under various cutting temperature.

Table 1. Parameters for Johnson-Cook and strain gradient material models. [28, 30]

| Material | A (MPa) | B (MPa) | n | C | m | $\dot{\varepsilon}_0$ (s$^{-1}$) | Tr (°C) | Tm (°C) | G (MPa) | b (mm) | α | μ | $\bar{r}$ |
|---|---|---|---|---|---|---|---|---|---|---|---|---|---|
| Ti-64 | 782.7 | 498.4 | 0.28 | 0.028 | 1 | 1e-5 | 20 | 1660 | 41097 | 2.95 e-7 | 0.5 | 0.38 | 1.0 |
| Copper | 90 | 292 | 0.31 | 0.025 | 1.09 | 1 | 20 | 1083 | 48000 | 2.56 e-7 | 0.5 | 0.38 | 1.85 |

# 3 Dislocation dynamics modeling for micro-cutting

## 3.1 Method of discrete dislocation dynamics

In order to reveal the motion and interaction of subsurface defects in the processing of micromechanical structures, a 2.5-dimensional dislocation dynamics-based multiscale framework was developed in Fig. 3. Two different spatial and temporal scales were incorporated into this procedure. For discrete module in mesoscale, a series of rules, algorithms and models associated with dislocations motion, collision and dissociation have been proposed. As dislocations move, they must overcome interior drag force and local Peierls lattice force. Furthermore, they may encounter various obstacles such as locks, defect clusters and elemental impurities.

The driving force of individual dislocation $i$ exerted by external loading could be calculated through the Peach-Koehler (P-K) force $f_i$.

$$f_i = ((\sigma^{applied} + \sigma^{interaction} + \sigma^{others}) \cdot b_i) \times \xi_i \tag{12}$$

where $b_i$ is the Burgers vector of dislocation $i$, $\xi_i$ is the line unit vector of dislocation $i$, $\sigma^{interaction}$ denotes the interaction force generated by other dislocation, $\sigma^{others}$ indicates the contribution of other damages and impurities, $\sigma^{applied}$ denotes applied stress field, which was obtained from continuum module by discrete-continuum method (DCM) [32]. In DCM coupling model, the intrinsic-stress captured by DDD code was subtracted to reveal the linear complementary stress $\sigma^{NOD}$ for individual node. Meanwhile, an interpolation algorithm was employed to transfer the driving stress into subsurface dislocations in micro-scale orthogonal machining.

The topology update of discrete dislocation network in DDD script could factually reflect the physics of dislocation interaction and accumulation. The Burgers vector actions (slip, climb, pile-up and annihilation) occur naturally through the evolution of dislocation nodes. Moreover, dislocation junction and cross-slip were programed to melt the 3-dimensional linear defect characteristics into 2-dimensional plane field, which further reinforced screw dislocation reaction. It is worth noting that present study would ignore the feature of twinning deformation due to high-level of Al element [33].

## 3.2 Model description

Based on the research of Thomas, dislocations multiplication and collision in alpha-titanium phase made up the elementary components of subsurface damaged layer in machining Ti-6Al-4V [11]. For simulating the equiaxed-axis alpha grains, polycrystalline Hexagonal-Close-Packed (HCP) structure is utilized in DDD simulation module. Due to the relatively low stacking fault energy of HCP crystal under investigation, the effect of stacking fault was inhibited. The dimensions of computational cell were 30 μm × 12 μm in volume. Meanwhile, homogeneous 3.4 μm × 2.95 μm HCP grains were built. The initial substrate structure was developed by inserting randomized pre-existing dislocations with density $6.25 \times 10^{12}$ m$^{-2}$ and F-R dislocation sources with density $4.2 \times 10^{13}$ m$^{-2}$ into representative cell. Similarly, dislocation obstacles with density $2.1 \times 10^{13}$ m$^{-2}$ for simulating nano-precipitates

scattered across glide planes. Partial material parameters of titanium alloy Ti-6Al-4V were utilized: vacancy energy of 2.509 eV, diffusion constant of 0.015 cm$^2$/s, drag coefficient of $1.4\times10^{-4}$ Pa·s, P-N force of 0.02 MPa. In addition, a uniform-sized micro-orthogonal cutting model was carried out to simulate the unsteady-state machining process. In this case, cutting edge radius was 0.25 μm, normal rake angle was 15° and flank angle was 6°. The chip morphologies depend on the chip separation criterion greatly. J-C shear failure model and Hillerborg's fracture energy were considered and introduced to concern the initiation and evolution of damage, respectively [34]. In conventional micro-cutting case, the adopted coefficient of friction was 0.47 in this model from Ref [35], which was derived from the experimental results. Moreover, heat generation conditions have been defined accordingly in order to permit the thermal interaction between workpiece material and tool. In present study, the thermal transfer coefficient was $4\times10^4$ W/m$^2$K, the friction energy transferred into heat was 100% and thermal partition coefficient was taken as 0.5. The strain gradient material equation was compiled by ABAQUS/VUHARD subroutine.
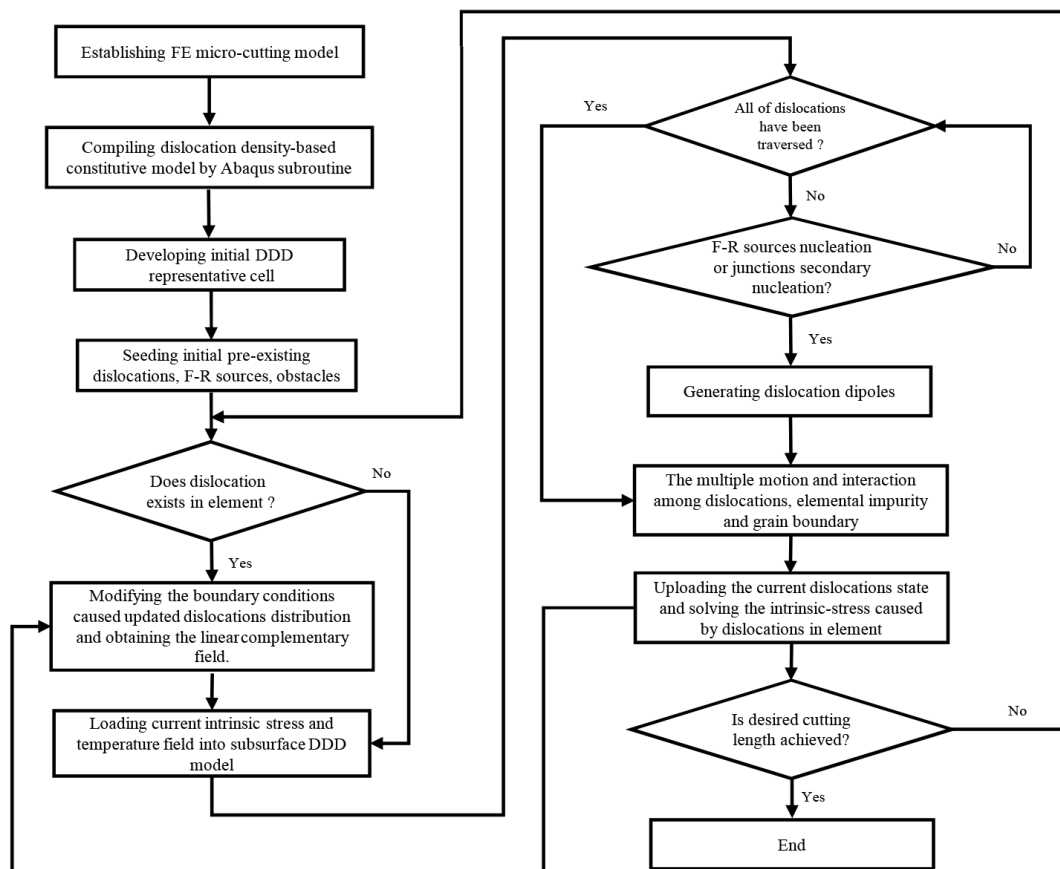


Figure 3. Flow chart for proposed modelling.

# 4 Results and discussion

In order to understand the formation mechanism and spatial arrangement of subsurface defects, a series of multiscale simulations of micro-cutting process have been performed. Particularly, two critical machining parameters, uncut chip thickness and cutting speed, were examined in detail because these factors would seriously affect the processing performance. Fig. 4 showed the simulated images of SSD layer under various undeformed chip thicknesses against cutting distance of 3 μm. As workpiece material was removed, the titanium alloy substrate generated surface metamorphic layer and subsurface SSD layer. Meanwhile, the comprehensive effect of residual stress and inner stress produced by prestored damages resulted in the proliferation and propagation of subsurface

dislocations. Over the course of defects generation, the morphologies of SSD layers were mainly affected by double behaviors, dislocation migration and dislocation climb. Intragranular dislocations slip and cross-slip motions were the dominant mechanism of parallel and intersecting dislocation arrays. Meanwhile, climb can be simply to make activation on all possible glide planes due to high stress and temperature level. Then, the edge and screw dislocations jump into neighboring planes and slip on these ones with short distances. Note that the spacing between activated slip planes was stabilized at 100$b$, but the climbing distance of unit dislocation segment must be subjected to the comprehensive influence of climb force, absolute temperature and vacancy formation energy.

According to the calculation results in Fig. 4, various uncut chip thicknesses resulted in distinct subsurface characteristics. When the depth of cut was 0.5 μm, loosely tangled dislocation patterns were found beneath finished surface. Due to the low penetrability of grain boundaries (GBs), mixed dislocation structure of blocked and gathered dislocation segments nearby GBs and obstacles were observed as well. As simulation goes on, above phenomena can result in the transformation of intracrystalline defects into subgrain boundaries [7]. Moreover, it should be noted that the accumulation organizations would fabricate cyclic subsurface hardening under fluctuating thrust cutting force [36]. With the augment of undeformed chip thickness, bulk materials have to take place dislocation nucleation in deep-surface to accommodate higher resolved shear stress. By contrasting subsurface patterns in Fig. 4a and Fig. 4d, the variation of SSD layer's thickness and area were extraordinary. It is readily seen that the depth of SSD layer went up 55.4 % and the area of SSD layer increased to 388.4 % when the depth of cut arrived at 3 μm. In addition, two regimes of subsurface morphologies were found in micro-cutting operations, which demonstrated distinct plastic deformation features from the top down, namely: (1) plenty of accumulated dislocations and refined crystal cells were generated in near-surface zone, and its thickness was equal to or near to the depth of cut. (2) the features within representative dislocation cell structures demonstrated the existence of persistent slip bands in deep-surface zone. These slip bands were composed primarily of ladder-shaped dislocation lines perpendicular to default <11-20> {10-10} glide system. It is well reminded that the extrusion and intrusion actions between high-density dislocation bands and low-density workpiece bulk would lead to the initiation of micro-crack.
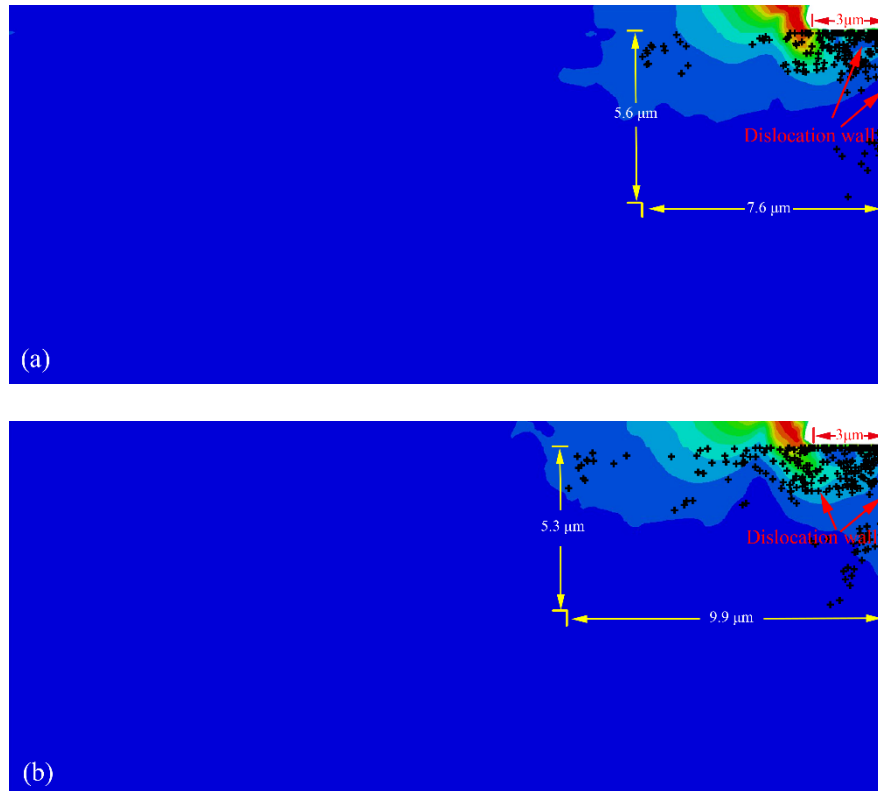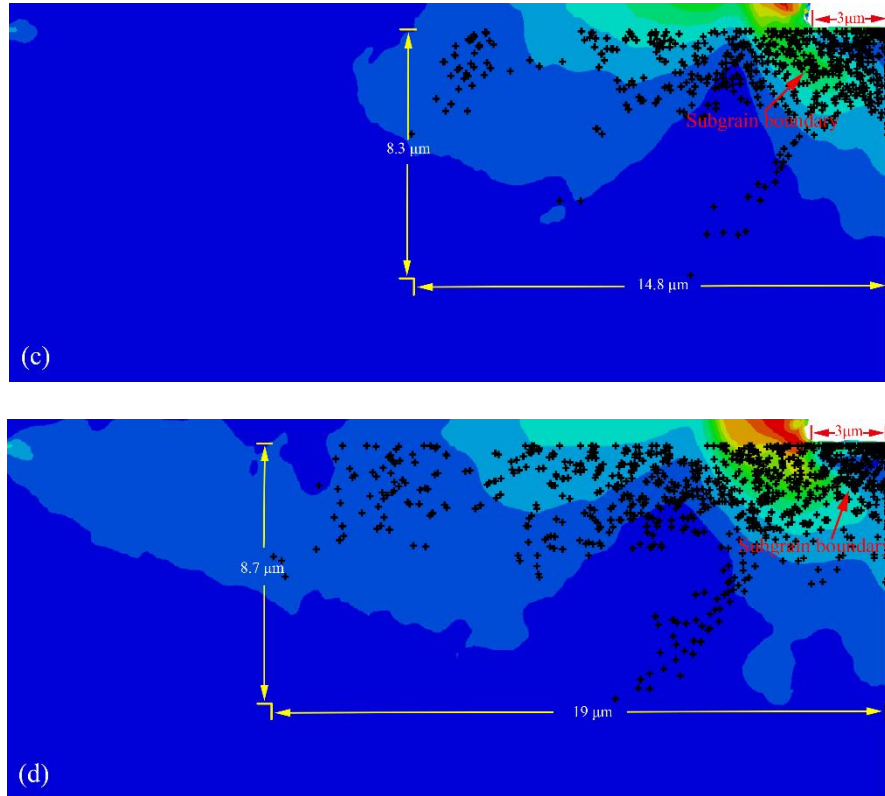
Figure 4. Simulation results of subsurface defects structure at various uncut chip thicknesses (a) a depth of cut 0.5 μm; (b) a depth of cut 1 μm; (c) a depth of cut 2 μm; (d) a depth of cut 3 μm. (cutting speed 600m/min and cutting length 3 μm).

To further quantitatively explore the generation of SSD layer in micro-machining of titanium alloy, the effect of cutting speed on dislocation morphologies was investigated in Fig 5. In comparison to previous MD studies, whose cutting speed stayed around 18000 m/min [37], the predictions matched well with actual operations. Results indicated that the subsurface microstructure exhibited hypersensitivity to increased cutting velocity. On the evolution of SSD layer, faster machining process can facilitate fewer subsurface defects. When the speed ranged from 600 to 2400 m/min, it is easy to get that the length and thickness of predicted subsurface damaged zone were off 54.7 % and 27.8 %, respectively. Meanwhile, dislocation's quantity was falling and the area of SSD layer declined 67.2 %. It can be explained that the very high cutting speed could lead to strong heating softening effect at near-surface area because of poor thermal conductivity of Ti-6Al-4V alloy, which significantly reduced cutting force and enormously boosted the climbing capability [38-40]. Climb mechanism is responsible for the promoted localized ductility of workpiece material by helping piled-up dislocations go on the lam. However, it is noteworthy that the excessive level of climb velocity would be attributed to the earlier appearance of dislocations accumulations around band-like intra-grain defects and GBs. Then, while the subsurface strain strengthening was more competitive than softening effect, the reduction of SSD layer area has been restrained, as shown in Fig. 5c and Fig. 5d.

Moreover, once the cutting speed beyond 1800 m/min, a fraction of initial dislocation sources has not enough time for nucleation. Subsequently, the limited subsurface structure generated continuous recrystallization and grain refinement. It is worth mentioning that above organizational change always results in the uncertain performance of finished component. Relative to ultrathin surface white layer, the effect of SSD layers on substrate properties played a greater role. For instance, the movable deep-surface dislocation bands would cause the hardness data of material raises before inhibition and even less than bulk material, which coincides well with former experimental testing [41].
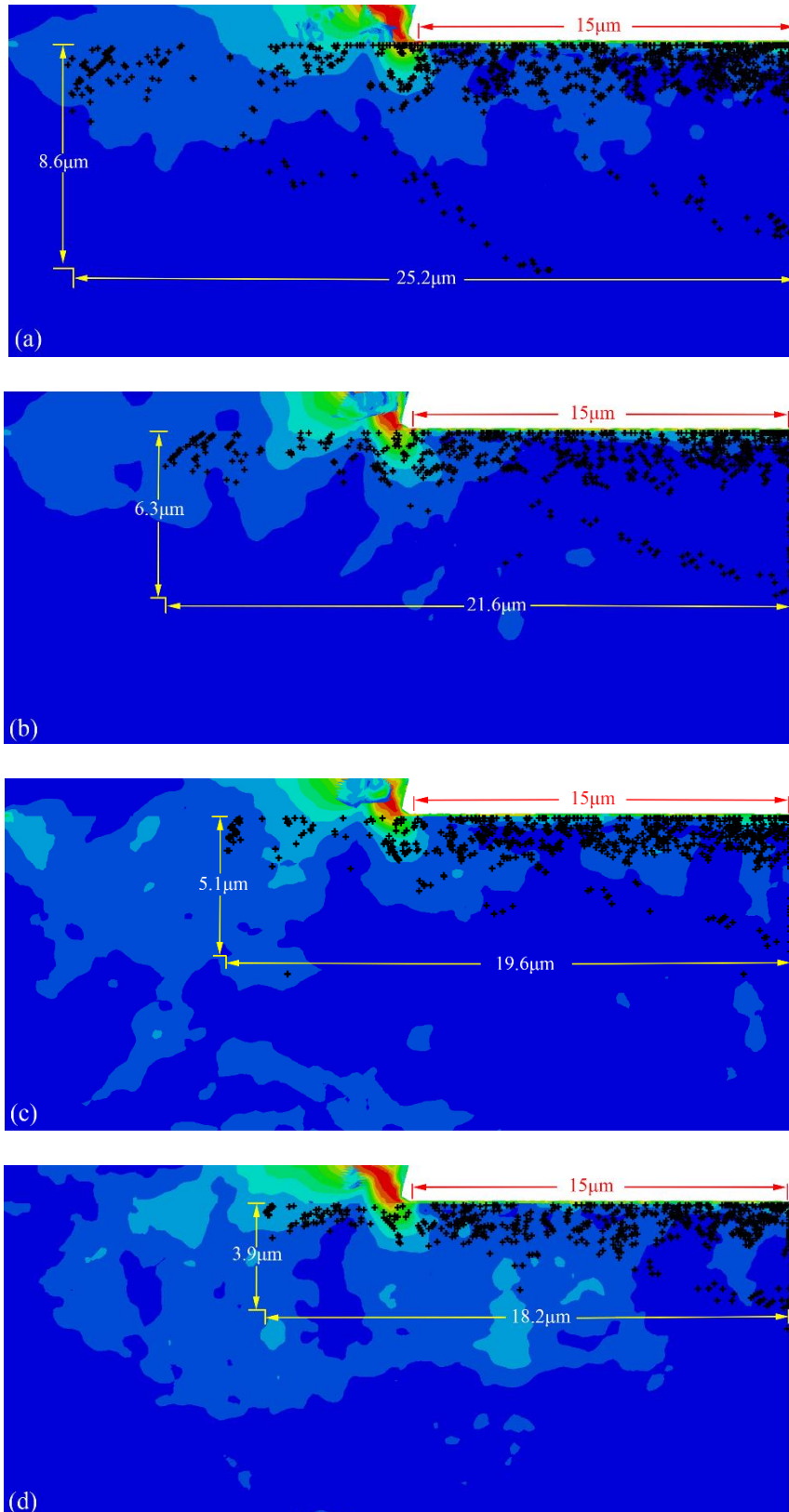
Figure 5. Simulation results of subsurface defects structure at various cutting speeds (a) a cutting speed of 600 m/min; (b) a cutting speed of 1200m/min; (c) a cutting speed of 1800m/min; (d) a cutting speed of 2400m/min. (cutting depth 1 μm and cutting length 15 μm).

# 5 Experimental validation

For investigating the predictions, a series of micro-milling tests were conducted. The microminiature experimental facility was displayed in Fig. 6a. The self-developed ultra-precision milling machine is composed of the linear axes of X, Y, Z, the rotational axes of B, C and motorized spindle. Polished titanium alloy Ti-6Al-4V bulk was cut into several 40 mm × 20 mm × 20 mm specimens. The average grain size of workpiece sample is 15 μm. Brand small granularity polycrystalline diamond (PCD) mills were adopted in this manuscript. Furthermore, the cutting tool diameter is 4.5 mm, the number of teeth is two, the cutting edge radius is 20 μm and the rake angle and clearance angle are 5° and 15°, respectively. The main and tip view images of PCD micro-end mill were shown in Fig. 6b. Varying uncut chip thicknesses and cutting velocities were proposed, which closely linked to feed rate, the depth of cut and spindle speed. Detailed processing parameters were indicated in Table. 2. After machining, the middle sections of milled micro-grooves were characterized by using X-ray diffraction (XRD, PANalytical, Almelo, the Netherlands) with Cu $K_\alpha$ radiation source.
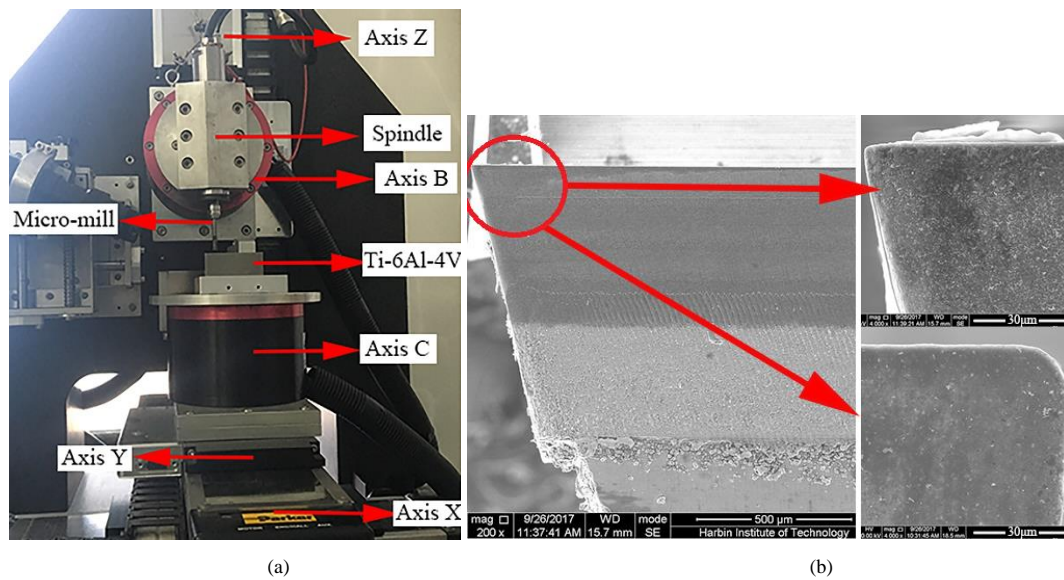


(a)                  (b)

Figure 6. Experimental setup (a) miniature milling machine; (b) the main and top views of brand PCD tool.

Table 2. Experimental matrix of micro-end milling of Ti-6Al-4V alloy.

| Test no. | Tool diameter (mm) | Cutting edge radius (μm) | Depth of cut $\alpha_p$ (μm) | Spindle speed $n$ (rpm) | Cutting speed $v$ (m/min) | Cutting distance $l$ (mm) |
|---|---|---|---|---|---|---|
| 1 | 4.5 | 20 | 15 | 25000 | 353.3 | 15 |
| 2 | 4.5 | 20 | 30 | 25000 | 353.3 | 15 |
| 3 | 4.5 | 20 | 60 | 25000 | 353.3 | 15 |
| 4 | 4.5 | 20 | 15 | 20000 | 282.6 | 15 |
| 5 | 4.5 | 20 | 15 | 15000 | 212.0 | 15 |

In comparison to general testing methods, XRD technique can spill over into the samples and exhibit subsurface information without introducing damages in the stage of sample preparation [42]. Not only that, the XRD diffraction signals would assert the detections of residual stress and microscopic stress of processed micro-slots subsurface. The presence of residual stress always induces the shifting of diffraction peaks of alpha-titanium to large angle or little angle. In contrast, the microscopic internal stress within grain and subgrain, generated by subsurface dislocations and distorting lattice, were embodied as reduction in diffraction peak intensity and augment in width. In terms of previous research, the more complicated subsurface damages microstructure, the

higher material internal stress [4]. Thus, by comparing various diffraction peak patterns, it is easy to characterize the variation mechanism of SSD layer during micro-end milling titanium alloy Ti-6Al-4V.

As shown in Fig. 7, the measurement of profiles was performed by varying two-theta from 20° to 60° with the step of 0.05° [43]. Meanwhile, the peak height, peak area and full width at half maximum (FWHM) were indexed. Fig. 8a reflected the XRD spectrum of original unfinished workpiece. Fig. 8 b-d demonstrated a series of differences in the magnitude of peak intensity with the increment of undeform chip thickness. As the depth of cut ranged from 15 μm to 60 μm, the value of FWHM increased from 0.323 to 0.350 as well. The experimental measurements kept consistent in former predictions, which confirmed that increased cutting depth produced irreversible impacts on bulk microstructure. Fig. 8e-f showed the contribution of cutting speed to SSD layer. As a finial note, although the peak height of diffraction patterns indicated a decrease when the cutting speed decreased to 212.0 m/min, the evolution law of FWHM values showed a certain deviation from above discussion. Actually, as asserted in section 4, surface grain refinement is sensitive to the orthogonal cutting speed. Excessive refined grains would result in the broaden of XRD diffraction peak as well. Therefore, Meanwhile, present numerical model has been shown as a computation-efficient tool to obtain the evolution of damages at SSD layer.
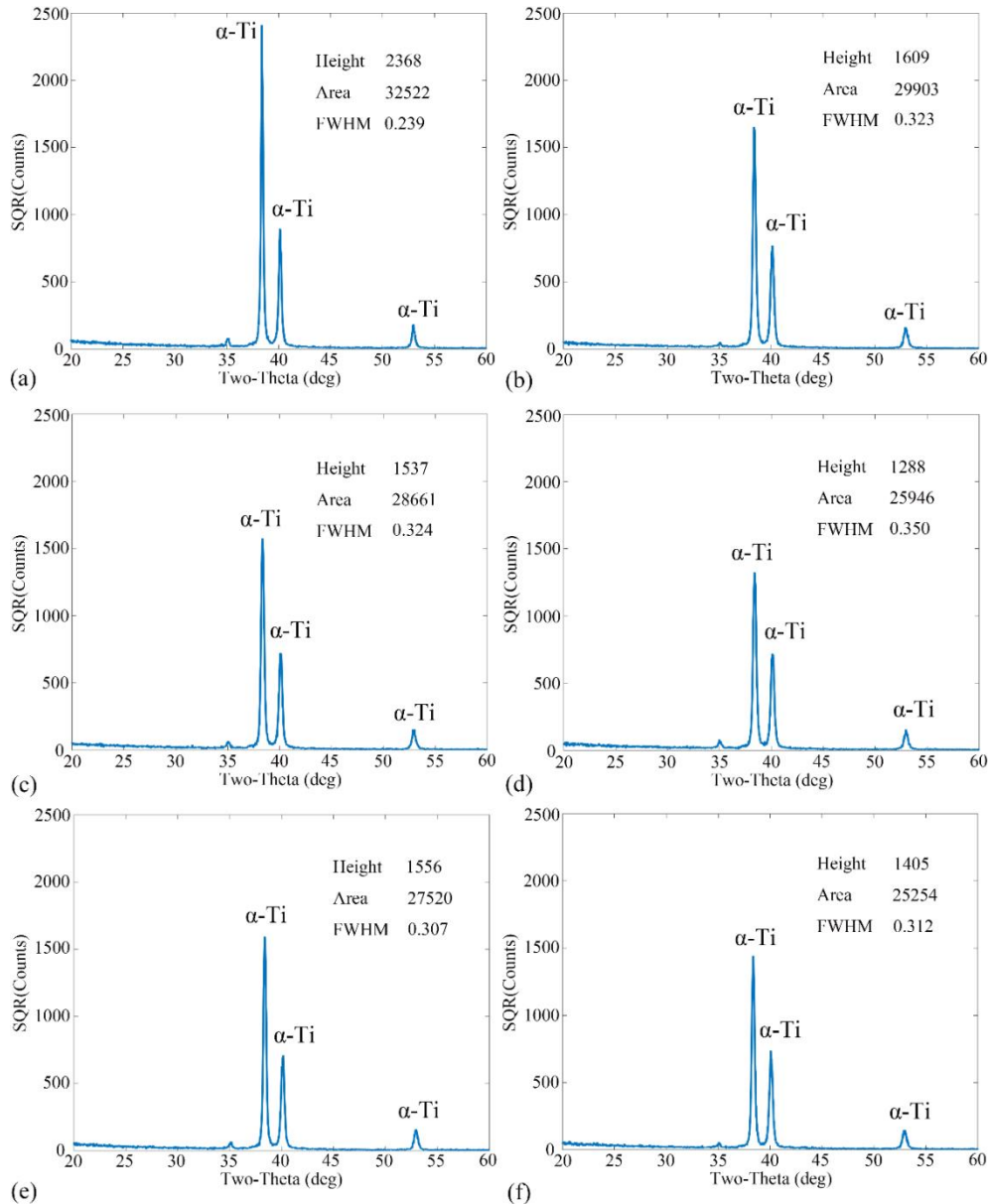
Figure 7. XRD patterns under various processing parameters (a) XRD spectrum of unfinished workpiece; (b)-(f) XRD spectrums of Test no.1-5.

## 6 Conclusions

In this paper, the essential characteristics of subsurface deformation field and microstructure transformation in orthogonal micro-cutting of Ti-6Al-4V alloy were successfully modeled using a DDD-based multiscale coupling framework. A discrete dislocation dynamics code has been developed to reveal the substrate damages multiplication and propagation during cutting. A dislocation density-based strain gradient numerical model was proposed to capture the linear complementary fields of subsurface defects. Present study paid an especial attention to the dependence of dislocation distributions on processing parameters particularly at SSD layer. In light of simulation results, selecting the smaller uncut cutting thickness and larger machining speed will contribute to obtaining an optimum subsurface microstructure. Two regimes of structural organizations were found, dislocation accumulations zone in near-surface and persistent slip bands zone in deep-surface, which lead to subsurface work hardening and bulk interior softening, respectively. Micro-milling and X-ray diffraction tests were conducted to validate the simulation results. Satisfactory conformance was obtained to confirm the physical predictions proposed to assess the SSD layer.

## Acknowledgments

## Conflicts of Interest

The authors declare no conflict of interest.

## References

1.     Nouari M, Makich H. Experimental investigation on the effect of the material microstructure on tool wear when machining hard titanium alloys: Ti-6Al-4V and Ti-555. Int J Refract Met H 2013; 41: 259-269.

2.     Mashinini PM, Dinaharan I, David Raja Selvam J, Hattingh DG. Microstructure evolution and mechanical characterization of friction stir welded titanium alloy Ti–6Al–4V using lanthanated tungsten tool. Mater Charact 139; 2018: 328-336.

3.     Bai JX, Bai QS, Tong Z. Dislocation dynamics-based modeling and simulations of subsurface damages microstructure of orthogonal cutting of titanium alloy. Micromachines 2017; 8: 309.

4.     Bai JX, Bai QS, Tong Z, Chen GD. The influence of cutting parameters on the defect structure of subsurface in orthogonal cutting of titanium alloy. J Mater Res 2018; 33: 720-732.

5.     Wang QL, Bai QS, Chen JX, Su H, Wang ZG, Xie WK. Influence of cutting parameters on the depth of subsurface deformed layer in nano-cutting process of single crystal copper. Nanoscale Res Lett 2015; 10: 396.

6.     Salahshoor M, Guo YB. Finite element simulation and experimental validation of residual stresses in high speed dry milling of biodegradable magnesium-calcium alloys. Int J Mech Sci 2014; 80: 153-159.

7.     Bai JX, Bai QS, Tong Z, Hu C, He X. Evolution of surface grain structure and mechanical properties in orthogonal cutting of titanium alloy. J Mater Res 2016; 31: 3919-3929.

8.     Gao Y, Urbassek HM. Evolution of plasticity in nanometric cutting of Fe single crystals. Appl Surf Sci 2014; 317: 6-10.

9. Yan JW, Asami T, Harada H. Crystallographic effect on subsurface damage formation in silicon microcutting. CIRP Ann - Manuf Tech 2012; 61: 131-134.

10. Ni H, Alpas AT. Sub-micrometer structures generated during dry machining of copper. Mat Sci Eng A 2003; 361: 338-349.

11. Thomas M, Turnerb S, Jackson M. Microstructural damage during high-speed milling of titanium alloys. Scripta Mater 2010; 62: 250-253.

12. Ginting A, Nouari M. Surface integrity of dry machined titanium alloys. Int J Mach Tool Manufact 2009; 49: 325-332.

13. Touazine H, Jahazi M, Bocher P. Accurate determination of damaged subsurface layers in machined Inconel 718. Int J Adv Manuf Technol 2017; 88: 3419-3427.

14. Dandekar CR, Shin YC. Multi-step 3-D finite element modeling of subsurface damage in machining particulate reinforced metal matrix composites. Compos Part A 2009; 40: 1231-1239.

15. Wang CC, Fang QH, Chen JB, Liu YW, Jin T. Subsurface damage in high-speed grinding of brittle materials considering kinematic characteristics of the grinding process. Int J Adv Manuf Technol 2016; 83: 937-948.

16. Bai JX, Bai QS, Tong Z. Experimental and multiscale numerical investigation of wear mechanism and cutting performance of polycrystalline diamond tools in micro-end milling of titanium alloy Ti-6Al-4V. Int J Refract Met H 2018; 74: 40-51.

17. Ding HT, Shen NG, Shin YC. Modeling of grain refinement in aluminum and copper subjected to cutting. Comp Mater Sci 2011; 50: 3016-3025.

18. Ding HT, Shin YC. Dislocation Density-Based Grain Refinement Modeling of Orthogonal Cutting of Titanium. J Manuf Sci E 2014; 136: 041003.

19. Wang QL, Bai QS, Chen JX, Sun YZ, Guo YB, Liang YC. Subsurface defects structural evolution in nano-cutting of single crystal copper. Appl Surf Sci 2015; 344: 38-46.

20. Pei QX, Lu C, Lee HP. Study of materials deformation in nanometric cutting by large-scale molecular dynamics simulations. Nanoscale Res Lett 2009; 4: 444-451.

21. Ren XD, Zhou WF, Ren YP, Xu SD, Liu FF, Yuan SQ, Ren NF, Huang JJ. Dislocation evolution and properties enhancement of GH2036 by laser shock processing: Dislocation dynamics simulation and experiment. Mat Sci Eng A 2016; 654: 184-192.

22. Zhang JL, Zaefferer S, Raabe D. A study on the geometry of dislocation patterns in the surrounding of nanoindents in a TWIP steel using electron channeling contrast imaging and discrete dislocation dynamics simulations. Mat Sci Eng A 2015; 636: 231-242.

23. Bai JX, Bai QS, Tong Z. Multiscale analyses of surface failure mechanism of single-crystal silicon during micro-milling process. Materials 2017; 10: 1424.

24. Wu JH, Liu ZQ. Modeling of flow stress in orthogonal micro-cutting process based on strain gradient plasticity theory. Int J Adv Manuf Technol 2010; 46: 143-149.

25. Swadener JG, George EP, Pharr GM. The correlation of the indentation size effect measured with indenters of various shapes. J Mech Phys Solids 2002; 50(4): 681-694.

26. Wang CL, Lai YH, Huang JC, Nieh TG. Creep of nanocrystalline nickel: A direct comparison between uniaxial and nanoindentation creep. Scripta Mater 2010; 62: 175-178.

27. Liu X, Melkote SN. Finite element analysis of the influence of tool edge radius on size effect in orthogonal micro-cutting process. Int J Mech Sci 2007; 49: 650-660.

28. Ding HT, Shen NG, Shin YC. Thermal and mechanical modeling analysis of laser-assisted micro-milling of difficult-to-machine alloys. J Mater Process Tech 2012; 212: 601-613.

29. Huo DH, Lin C, Choong ZJ, Pancholi K, Degenaar P. Surface and subsurface characterisation in micro-

milling of monocrystalline silicon. Int J Adv Manuf Technol 2015; 81:1319–1331.

30.    Ding HT, Shen NG, Shin YC. Modeling of grain refinement in aluminum and copper subject to cutting. Comp Mater Sci 2011; 50: 3016-3025.

31.    Arsenlis A, Parks DM. Crystallographic aspects of geometrically-necessary and statistically-stored dislocation density. Acta Mater 1999; 47: 1597-1611.

32.    Huang MS, Li ZH. Coupled DDD-FEM modeling on the mechanical behavior of microlayered metallic multilayer film at elevated temperature. J Mech Phys Solids 2015; 85: 74-97.

33.    Fernandez-Zelaia P, Melkote S, Marusich T, Usui S. A microstructure sensitive grain boundary sliding and slip based constitutive model for machining of Ti-6Al-4V. Mech Mater 2017; 109: 67-81.

34.    Zhang YC, Mabrouki T, Nelias D, Gong YD. Chip formation in orthogonal cutting considering interface limiting shear stress and damage evolution based on fracture energy approach. Finite Elem Anal Des 2011; 47: 850-863.

35.    Dandekar CR, Shin YC, Barnes J. Machinability improvement of titanium alloy (Ti–6Al–4V) via LAM and hybrid machining. Int J Mach Tool Manu 2010; 50: 174-182.

36.    Gaudin C, Feaugas X. Cyclic creep process in AISI 316L stainless steel in terms of dislocation patterns and internal stresses. Acta Mater 2004; 52: 3097–3110.

37.    Wang QL, Bai QS, Chen JX, Su H, Wang ZG, Xie WK. Influence of cutting parameters on the depth of subsurface deformed layer in nano-cutting process of single crystal copper. Nanoscale Res Lett 2015; 10: 396.

38.    Sutter G, List G. Very high speed cutting of Ti–6Al–4V titanium alloy - change in morphology and mechanism of chip formation. Int J Mach Tool Manu 2013; 66: 37-43.

39.    Gente A, Hoffmeister HW. Chip formation in machining Ti6A14V at extremely high cutting speeds. CIRP Ann 2001; 50: 49-52.

40.    Barry J, Byrne G, Lennon D. Observations on chip formation and acoustic emission in machining Ti–6Al–4V alloy. Int J Mach Tool Manu 2001; 41: 1055-1070.

41.    Sun J, Guo YB. A comprehensive experimental study on surface integrity by end milling Ti–6Al–4V. J Mater Process Tech 2009; 209: 4036-4042.

42.    Jia W, Peng ZN, Wang ZJ, Ni NC, Wang CY. The effect of femtosecond laser micromachining on the surface characteristics and subsurface microstructure of amorphous FeCuNbSiB alloy. Appl Surf Sci 2006; 253: 1299-1303.

43.    Palaniappan K, Murthy H, Rao BC. Production of fine-grained foils by large strain extrusion-machining of textured Ti-6Al-4V. J Mater Res 2018; 33: 108-120.